BCSJ Award Article

Chemistry of Anthracene–Acetylene Oligomers. XIX. Construction of Higher 1,8-Anthrylene–Alkynylene Macrocycles: Synthesis, Structures, and Conformational Analysis of Cyclic Hexamer and Dodecamer[1]

Shinji Toyota,* Hiroaki Harada, Hiroaki Miyahara, Takahiro Kawakami, Kan Wakamatsu, and Tetsuo Iwanaga

Department of Chemistry, Faculty of Science, Okayama University of Science, 1-1 Ridaicho, Kita-ku, Okayama 700-0005

Received April 27, 2011; E-mail: stoyo@chem.ous.ac.jp

Macrocyclic 1,8-anthrylene hexamer and dodecamer with acetylene and diacetylene linkers were synthesized by the metal-catalyzed cyclization of an acyclic hexamer with terminal alkyne units, and characterized by NMR and mass spectroscopy. The structure and conformational mobilities of their macrocyclic frameworks were analyzed by DFT calculations and ^{1}H NMR spectroscopy. The cyclic hexamer takes various parallelogram structures with the diacetylene linkers located at various positions, and those structures interconvert rapidly on the NMR time scale. The dodecamer tends to exist as highly folded structures that undergo exchange between several conformations rather slowly at room temperature. The intramolecular $\pi\cdots\pi$ interactions between anthracene units have a distinct effect on the structural features as well as the electronic spectra.

We have constructed several oligomers with anthrylene units and ethynylene (or butadiynylene) linkers to create new types of arylene–ethynylene oligomers possessing interesting structures and properties.[2] This molecular design has enabled us to construct various architectures by changing the number and substitution position of anthracene units as well as the combination of the two linkers.[3] The first key compound in our series of studies is 1,8-anthrylene cyclic tetramer **1** (Figure 1), which features a diamond prism structure stabilized by intramolecular $\pi\cdots\pi$ interactions and the dynamic behavior of skeletal rocking caused by conformational changes about the acetylene axes.[4] The synthesis of large cyclic oligomers is vital to further diversify the scope of oligomer chemistry. As proof of efforts to this end, we have recently reported the syntheses of cyclic hexamer and higher oligomers **2**–**5**,[1,5] which are characteristic as π-conjugated belt-shaped molecules.[2b–2d,6] In contrast to tetramer **1**, these compounds have several degrees of freedom in their macrocyclic frameworks, effectively forming a large number of molecular shapes. Spectroscopic and theoretical studies have revealed that these macrocycles generally take flat or folded conformations and undergo rapid interconversion between possible conformations in solution, although conformational analyses are not always straightforward. We needed to obtain large quantities of the final oligomers with tolerable stability and solubility to facilitate experiments aimed at structural and dynamic studies. Therefore, we synthesized

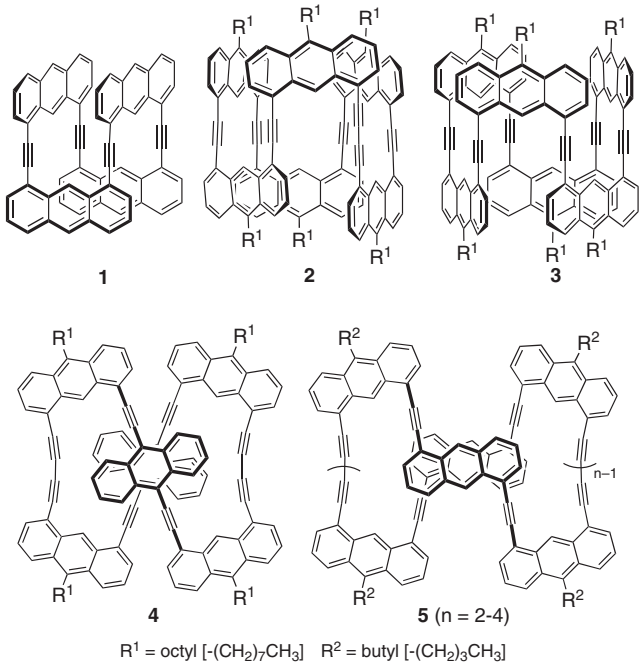

Figure 1. Anthrylene–alkynylene cyclic tetramer and higher oligomers reported in previous papers.

Published on the web July 21, 2011; doi:10.1246/bcsj.20110121

hexamer **6** (Figure 2), which is a modified version of hexamer **3** with two diacetylene linkers, because the diyne linkage by oxidative coupling usually gives better results than the monoyne linkage by the Sonogashira coupling for macrocyclization. Actually, the coupling of a hexameric precursor with terminal ethynyl groups afforded not only desired cyclic hexamer **6** (46-membered ring) but also double-sized macrocyclic product **7** (92-membered ring). We herein report the synthesis and properties of these macrocyclic products and discuss their structures and conformational flexibilities on the basis of spectroscopic measurements and structural calculations. In particular, we demonstrate that the DFT calculation with M05 functional gives valuable information on the structures of such large molecules with reasonable reliability.

Results and Discussion

Synthesis and Characterization. The target compounds were synthesized via the route shown in Scheme 1. An alkyl group was introduced at the 10-position of the central anthracene group in trimeric precursor **11** to increase solubility. Preliminary experiments revealed that an octyl group that had been adopted in the synthesis of **2**–**4**[1,5] was not sufficient to enhance the solubility for purification and spectroscopic measurements. One possible way to enhance the solubility might be to introduce alkyl groups to more anthracene units. However, this approach was not practical for the synthesis of building units. Therefore, we adopted a longer alkyl group, a dodecyl group, as R in the target cyclic oligomers for practical reasons. We initially carried out the cyclization of the fully desilylated derivative of acyclic trimer **11**, which had been used as a versatile precursor for the synthesis of various oligomers.[4,7] However, we obtained not cyclic hexamer **6** but a small amount of cyclic trimer, an intramolecular cyclization product, and unidentified products. Hence, we needed to use an acyclic hexamer as the cyclization precursor.

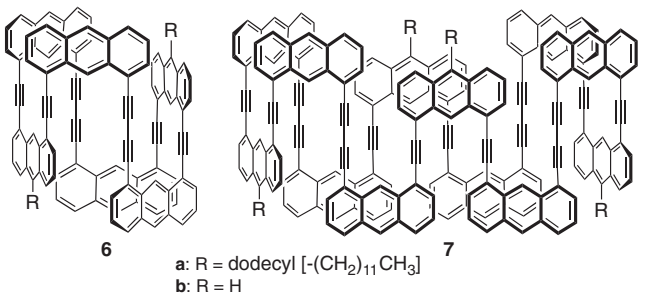

Figure 2. Target anthrylene–alkynylene macrocyclic oligomers **6** and **7**.

Diiodoanthracene **9** was prepared from 4,5-diiodo-9-anthrone (**8**)[8] and dodecylmagnesium bromide in an ordinary manner.[9] The Sonogashira coupling of **9** and diethynylanthracene **10** in a 1:2 ratio afforded trimer **11** in 78% yield. Compound **11** was treated with tetrabutylammonium fluoride (TBAF) in dichloromethane and singly desilylated product **12** was separated by chromatography. Trimer **12** was dimerized by Pd-catalyzed oxidative coupling to give hexamer **13**.[10] Compound **13** was fully desilylated with TBAF in THF and the formed terminal alkyne was treated with $Cu(OAc)_2$ and CuCl in pyridine under modified conditions for Eglington coupling.[10b,11] The crude products were separated by chromatography and recrystallization to give 20% of cyclic hexamer **6a** and a small amount of cyclic dodecamer **7a** both as yellow

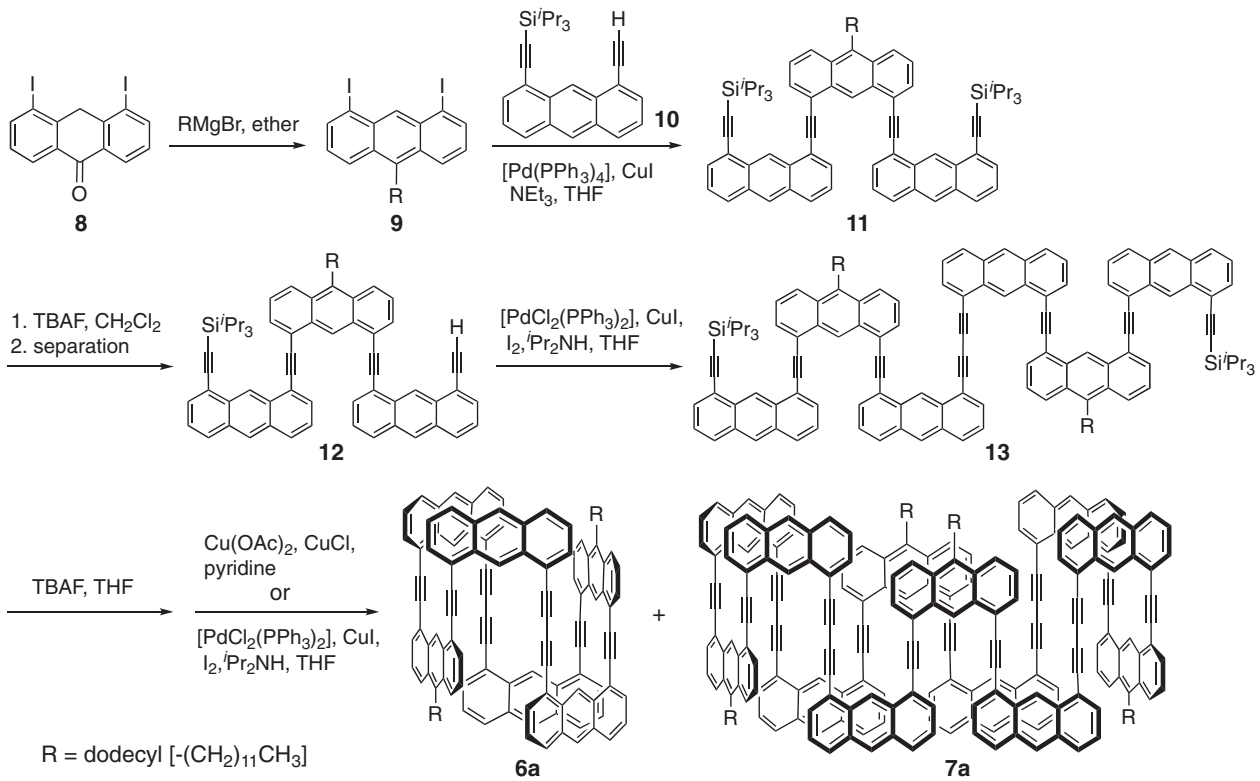

Scheme 1. Synthesis of cyclic oligomers **6a** and **7a**.

solids. Compounds **6a** and **7a** were formed by intramolecular cyclization and dimerization followed by macrocyclization, respectively. Their yields were not affected so much by the concentration and temperature of the reaction mixture. To obtain a larger amount of the cyclic dodecamer, we carried out the macrocyclization by oxidative Pd-catalyzed coupling with I_2 as oxidant to give **6a** and **7a** in 22 and 7% yields, respectively.[10] It was reported that the two conditions influenced the mode of ring closure of ethynylbenzene derivatives depending on the geometric requirement of the metal alkyne intermediate.[12] Such effect, however, is insignificant for the macrocyclization of the desilylated terminal alkyne of **13**. The increased yield of **7a** by the Pd-catalyzed coupling is attributed to the treatment during the purification step rather than the selectivity of the macrocyclization itself. Whereas hexamer **6a** is stable in the dark in a closed flask at room temperature, it slowly decomposes in organic solvents, such as chloroform, dichloromethane, and THF. Dodecamer **7a** is less stable than **6a** and decomposes significantly in solution during chromatography and recrystallization.

Cyclic oligomer **6a** gave a molecular ion peak at m/z 1584.7491 in the high-resolution FAB spectrum and this value is consistent with the molecular formula $C_{124}H_{96}$. Meanwhile, because **7a** afforded no molecular ion peaks under the same conditions, we measured its MALDI-TOF mass spectrum (Figure 3). The molecular ion peak of the largest intensity, $[M + 2]^+$, was observed at 3171.84, which was in agreement with the calculated value for $C_{248}H_{192}$. The isotope pattern of the observed peaks was reasonably reproduced by the calculation of the natural abundance of isotopes. The ^{1}H NMR signals of the oligomers became simple upon macrocyclization, evidencing the formation of cyclic structures (Figure 4). Both cyclic oligomers gave three pairs of ABC systems in a 1:1:1 ratio and three singlets due to 9,10-H in a 2:2:1 ratio in the aromatic region, although the signals were somewhat broad for dodecamer **7a** at room temperature. The structures of **6a** and **7a** have C_{2h} and D_{2d} symmetries, respectively, on the NMR time scale. It is noteworthy that some aromatic proton signals shifted upfield for the cyclic oligomers as well as the acyclic oligomers. For example, a double-doublet signal of **6a** was observed at δ 6.45, which is higher by ca. 1 ppm than those of ordinary aromatic protons. Whereas the signals due to 1-methylene protons in dodecyl groups appeared at δ 3.68 for the acyclic trimers, the corresponding signals shifted upfield to

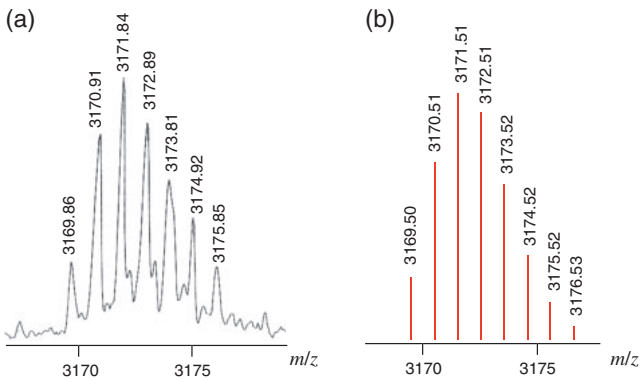

Figure 3. MALDI-TOF mass spectrum of cyclic dodecamer **7a** (a) and calculated isotope pattern for $C_{248}H_{192}$ (b).

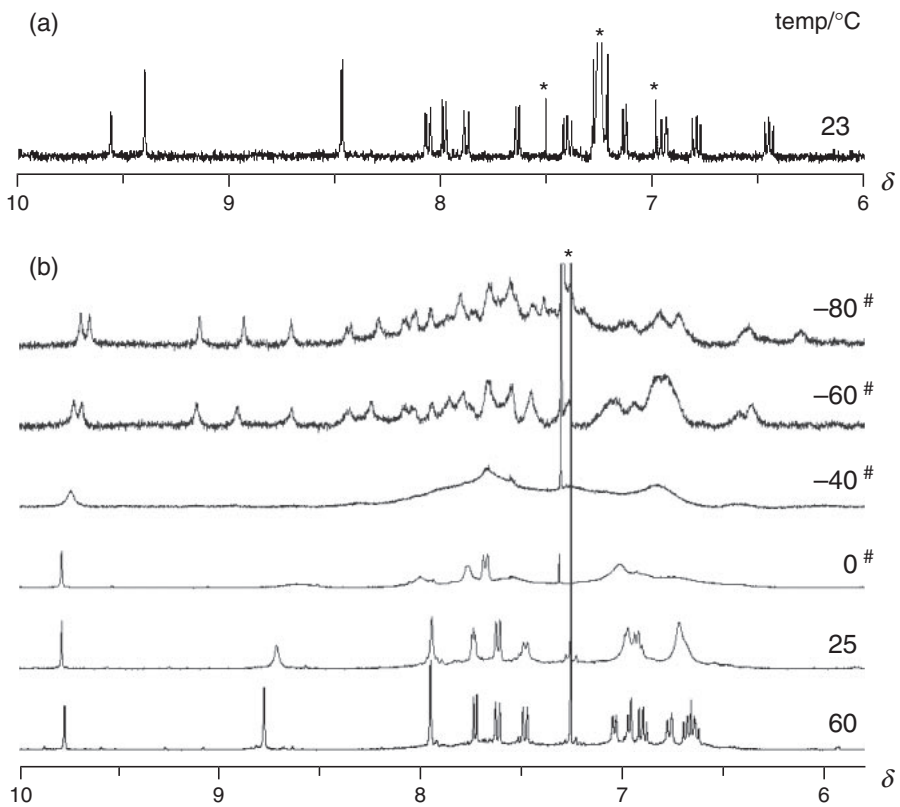

Figure 4. ^{1}H NMR spectra of hexamer **6a** (a) and dodecamer **7a** (b) in $CDCl_3$ or CD_2Cl_2 (#). *: signals due to solvent.

δ 2.2 and 1.6 for **6a** and **7a**, respectively. These protons are located in the shielding region of the anthracene moieties in the cyclic structures. These spectroscopic data will be discussed later in terms of the molecular structure. Unfortunately, the solubilities of **6a** and **7a** were too low to allow measurement of their ^{13}C NMR spectra.

Electronic Spectra. The UV–vis and fluorescence spectra of the cyclic oligomers and their precursor are shown in Figure 5. Absorption bands in the p-band region were observed in the range of 350–480 nm. Peaks at the longest wavelength were observed at ca. 460 nm for the cyclic oligomers, which was longer by 10 nm than the corresponding peak of **13**. Hence, the effects of ring size on the wavelength are small for the hexamers and the dodecamer, whereas the latter gave intense bands depending on the number of anthracene chromophores. Other hexamers **2a** and **3a** also afforded peaks at ca. 460 nm,[5]

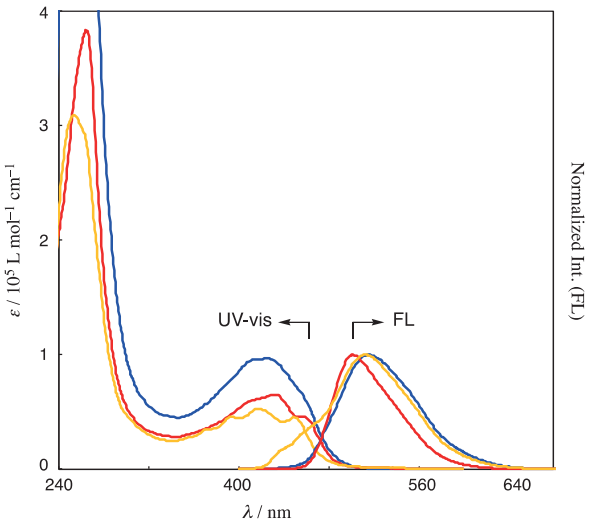

Figure 5. UV–vis and fluorescence spectra of cyclic oligomers **6a** (red) and **7a** (blue) and their precursor **13** (yellow) in $CHCl_3$.

and this means that the wavelength is not affected so much by the kind of linkers in the hexameric cyclic structures.

In the fluorescence spectra measured in $CHCl_3$, the emission peaks were observed at 502 and 516 nm for **6a** and **7a**, respectively, as broad bands. The fluorescence quantum yields Φ_f are 0.10 and 0.04 for **6a** and **7a**, respectively. These Φ_f values are comparable to those of hexamers **2a** (0.13) and **3a** (0.07),[5] and smaller than those of tetramers (0.20–0.40).[4,7a] The weak and broad emission bands of the macrocyclic oligomers are attributable to the intramolecular $\pi\cdots\pi$ contacts of the anthracene moieties,[13] because this phenomenon is known to be significant for some cyclophane π systems.[14] Such interactions occasionally lead to the appearance of long-lived emissions due to excimer formation as observed for cyclic tetramer **1** and its analogs. Unfortunately, fluorescence lifetime measurements revealed that the emission bands of the two cyclic oligomers consisted of one decay component of short lifetime (τ_f 4.5 ns).

Molecular Structure. Because we could not obtain single crystals suitable for X-ray analysis, we explored the molecular structures of the macrocyclic oligomers by theoretical calculations. We calculated the structures of **6b** without alkyl groups by DFT at the M05/3-21G level,[15] because this density functional and basis set provided good performance for other macrocyclic anthrylene–ethynylene oligomers.[1,5,7a] We optimized the structures from various conformations because this framework had three degrees of freedom. We obtained three parallelogram prism structures (Figure 6) as energy minima rather than hexagonal, triangular, rectangular, or other prism structures, as found for hexamers **2** and **3**.[5] The linker moieties are practically linear in all the structures: the bond angles at most of the sp carbons are larger than 175°. These parallelogram structures differ in the positions of the diacetylene linkers at obtuse angle corners (**A**), acute angle corners (**B**), and midpoints of long sides (**C**). All these structures have approximately C_i symmetry with one center of symmetry. Structure **A** is the global minimum and structures **B** and **C** are

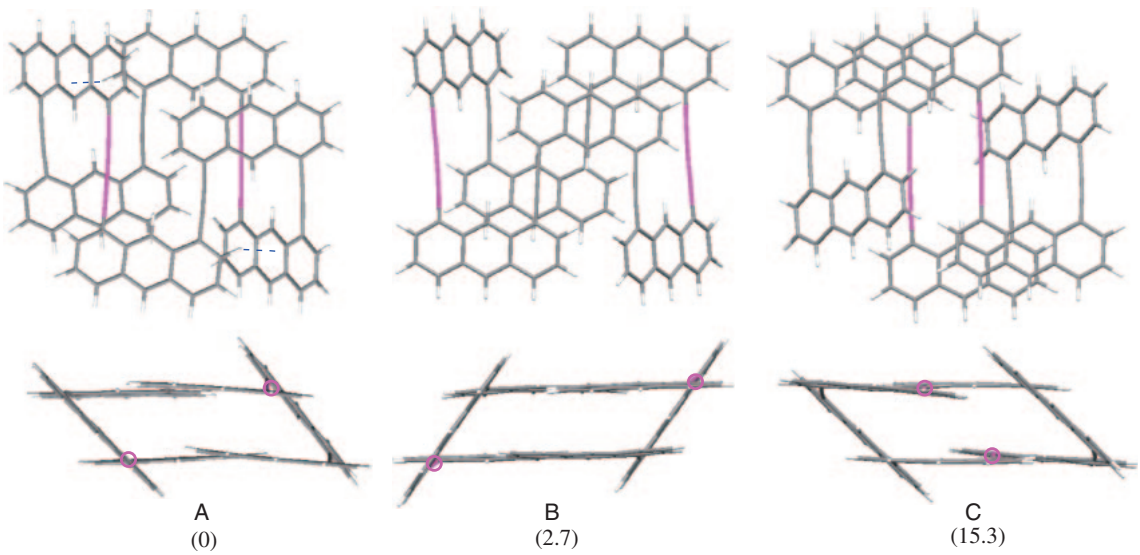

Figure 6. Two views of three optimized structures of **6b** at M05/3-21G level. Diacetylene linkers are indicated by magenta lines or circles. Important C–H$\cdots\pi$ contacts are shown as blue dashed lines. Relative energies are given in parentheses in kJ mol^{-1}.

less stable by 2.7 and 15.3 kJ mol^{-1}, respectively, than **A**. In **A** and **B**, the anthracene units attaching to two acetylene linkers (AA) on the long sides of the parallelogram face the diacetylene linkers and the acetylene linkers on the other long sides, respectively (Chart 1 for abbreviations of AA and AD). In **C**, there are two pairs of partial stacking between the anthracene units attaching to one acetylene linker and one diacetylene linker (AD) on the long sides. The distances of these intramolecular contacts are in the range of 3.3–3.5 Å, which are comparable to the sum of the van der Waals radii of sp^2 or sp carbons.[16] These $\pi\cdots\pi$ interactions play an important role in the preference for the parallelogram structures over other structures, as they can maximize attractive interactions. There are notable intramolecular C–H$\cdots\pi$ (anthracene) contacts at ca. 2.5 Å, as indicated in the structure of **A** in Figure 6.[17] The thus calculated conformational stability of **6b** well explains the upfield shift of the signals due to 1-methylene protons in dodecyl groups in **6a** mentioned above. In structures **A** and **B**, 10-H atoms in the AA units, which are replaced by dodecyl groups in **6a**, are in the shielding region of the stacking anthracene units.

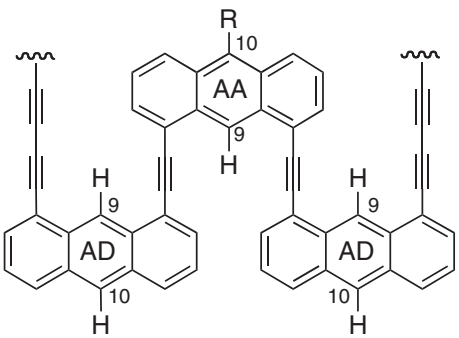

Chart 1.

We managed to calculate the structure of dodecamer **7b** at the same level despite its large molecular size. The possible conformations were not always fully searched because this framework, in principle, had nine degrees of freedom. We obtained three structures as shown in Figure 7. In most stable structure **D**, the three diacetylene corners are internally folded and there are two pairs of four-layered anthracene stackings and two pairs of two-layered stackings in addition to several C–H$\cdots\pi$ contacts. In this conformation, 10-H atoms in the AA units are located in the shielding region of the stacking anthracene units, being consistent with the upfield shift of the alkyl signals in the ^{1}H NMR spectrum of **7a**. Structure **E**, which is less stable by 24 kJ mol^{-1} than **D**, has four diacetylene linkers at the internally folded corners and four pairs of three-layered and partially stacked anthracene units. Its framework is slightly deformed from the D_2 symmetry and some acetylene carbons have bond angles smaller than 175°. Structure **F**, the least stable one, takes a long rectangle-like shape with two AA units at the short sides. One can find five pairs of stacked anthracene units along the long sides. The distances between stacking anthracenes are 3.5–3.6 Å in the all cases, which are slightly longer than those observed for the hexamer. These results mean that the molecules tended to take highly folded conformations rather than extended conformations.

Dynamic Behavior. To observe dynamic processes, the ^{1}H NMR spectra of the cyclic oligomers were measured at variable temperatures (Figure 4). Compound **6a** gave symmetric signals at room temperature and this signal pattern was maintained even at −60 °C in $CDCl_3$. Measurements at lower temperature in CD_2Cl_2 or other solvents were obstructed by low stability or solubility. If the molecules of **6a** were fixed in either of the parallelogram structures, the ^{1}H NMR spectra would be less symmetric than that observed. The averaged NMR signals at −60 °C indicate rapid exchanges between possible parallelogram conformations on the NMR time scale.

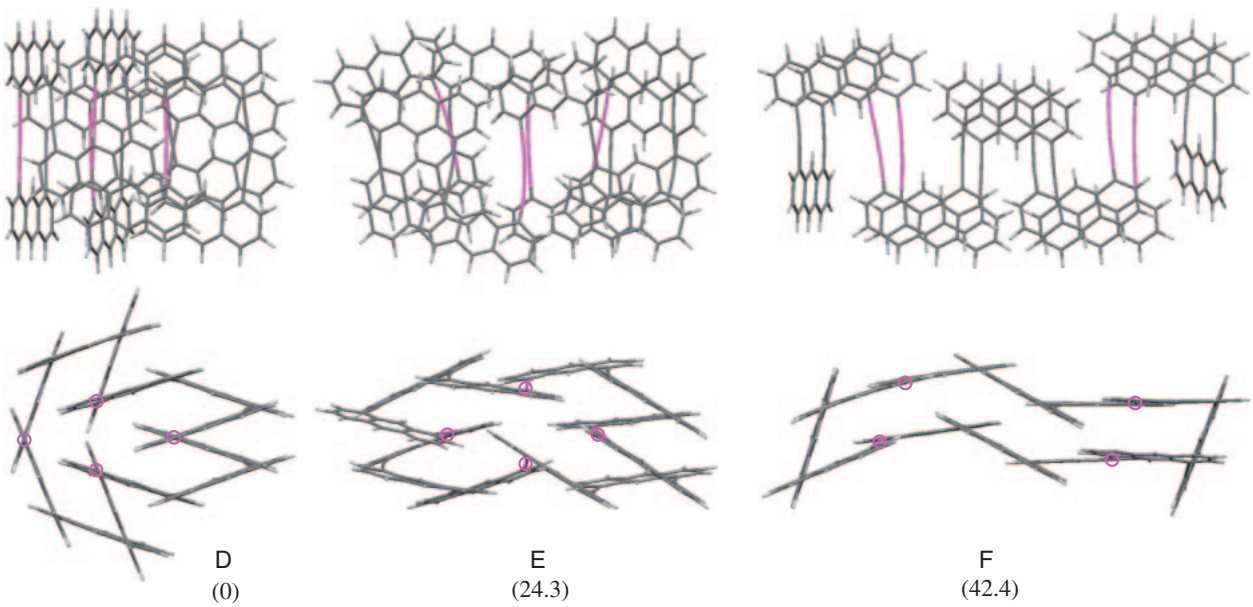

Figure 7. Two views of three optimized structures of **7b** at M05/3-21G level. Diacetylene linkers are indicated by magenta lines or circles. Relative energies are given in parentheses in kJ mol^{-1}.

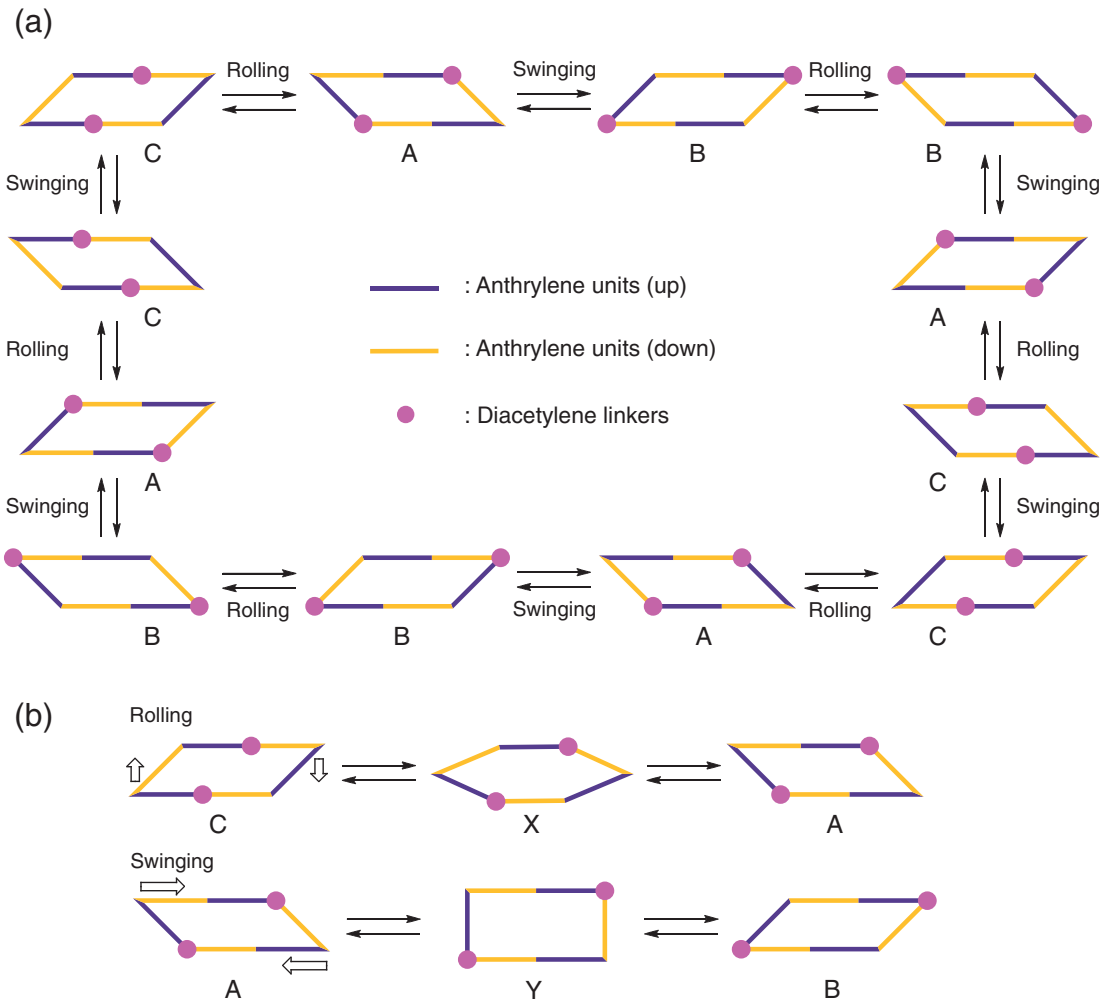

Scheme 2. Schematic of conformational circuit between parallelogram structures of **6** (a) and plausible transient structures of rolling and swinging process (b). Symbols **A**–**C** correspond to the structures in Figure 6.

A plausible exchange process is illustrated in Scheme 2a, which consists of two types of conformational changes between parallelogram structures. One is the swinging process that only exchanges the acute and obtuse angle corners mutually, and the other is the rolling process that changes the corner positions and the combination of the opposite sides. These processes can occur continuously to yield a dynamic circuit around all the 12 possible parallelogram structures. In one circuit, the same structures (topomers and homomers) appear four times for each conformational isomer. It was difficult to estimate the transition state and the activation energy for the elemental steps by the theoretical calculations. Analysis with the CPK molecular model demonstrated that the swinging motion should require a larger energy than the rolling motion because the former should take place via a rectangular conformation **Y** with less effective $\pi\cdots\pi$ stacking (Scheme 2b). Meanwhile, the rolling motion can take place while retaining the folded structures **X**. Therefore, the actual molecules rapidly undergo a series of caterpillar-like motions on the NMR time scale.

The proton signals of dodecamer **7a** were slightly broad at 25 °C in $CDCl_3$, and became sharp at 60 °C (Figure 4b). When the temperature was lowered in CD_2Cl_2, the signals considerably broadened, and the signals resharpened into several peaks at −60 °C and lower temperature. For example, the singlet at δ 9.8 split into at least two peaks and the singlets at δ 7.9 and 8.8 split into several peaks, even though the exchange was not completely frozen at −80 °C. These complicated line shape changes mean that conformational exchanges take place on the NMR time scale at low temperature. One possibility is the exchanges between several macrocyclic conformers via rotation about the acetylene linkers, and the other is the restricted rotation of the dodecyl groups relative to the anthracene groups. The calculated energies in Figure 7 mean that most of the molecules should exist as conformation **D**. To understand the observed line shape changes of **7a**, the expected signal patterns of the aromatic protons are counted based on the molecular symmetry (Table 1). Structure **D** should give two signals due to 9-H atoms in the AA units at the lowest magnetic field, four signals due to 9-H atoms in the AD units, and 12 sets of ABC systems. The ^{1}H NMR spectrum at the lowest temperature in Figure 4 is approximately consistent with this signal pattern rather than those for structures **E** and **F** of higher symmetries. The symmetric spectral pattern at 60 °C is explained by facile exchanges between four possible topomers of **D**, which differ in the internal folding position (Scheme 3). The average of the four structures is equivalent to the dynamic

symmetry of D_{4d} as indicated by **G** in Table 1. However, it is not straightforward to follow the conformational pathway from one structure **D** to another from available data. A plausible pathway via **E** as intermediate is shown in Scheme 3. Structure **D** can change into **E** by movement of the outside diacetylene corner to inward of the framework. The reverse process from **E** or its topomer, which is exchangeable by recombining stacked anthracene pairs, leads to any of the four structures of **D**. The observed spectra indicate that the exchanges were not sufficiently rapid even at room temperature and the rate of exchange should be of order $10^2\,s^{-1}$, corresponding to a barrier in the range of 55–60 kJ mol^{-1}. This barrier is clearly higher than that for the skeletal swing in cyclic tetramer **1** (38 kJ mol^{-1}),[4] which is mainly attributed to two pairs of $\pi\cdots\pi$ stacking of anthracene units. Therefore, the conformational exchanges of the dodecamer system involve both dissociation and association of weak interactions between building units, in particular $\pi\cdots\pi$ interactions, at multiple sites, resulting in an enhanced barrier.

Table 1. Expected Numbers of Signals Due to Aromatic Protons in the Calculated Structures of **7b**[a)]

Structure[b)]	Symmetry[c)]	9-H (AA)	9-H (AD) or 10-H (AD)	ABC (AA)	ABC (AD)
D	C_2	2	4	4	8
E	D_2	1	2	2	4
F	C_{2v}	2	2	2	4
G	D_{4d}	1	1	1	2

a) AA and AD: positions of anthracene units (see Chart 1 and text). ABC: signals due to anthracene protons at 2–7 positions observed as ABC systems. The conformation of the dodecyl groups is not considered in this analysis. b) **D**–**F**: calculated structures in Figure 7. **G**: average of all possible conformations. c) Approximate symmetry (point group) of the calculated structures and the averaged structure. Structure **F** is assumed to be a regular rectangular shape.

Conclusion

In conclusion, we have synthesized and spectroscopically characterized macrocyclic anthracene hexamer and dodecamer having acetylene and diacetylene linkers. The macrocyclic framework of these oligomers can take several conformations without significant strain because of rotational freedom about the linker moieties, as revealed by DFT calculation, which is a powerful tool for the structural analysis of large oligomers. Whereas the hexamer undergoes rapid exchanges between several parallelogram-shaped conformations, similar to a caterpillar, the dodecamer undergoes relatively slow exchanges between several highly folded structures. These structural and dynamic features are mainly attributed to intramolecular interactions, especially $\pi\cdots\pi$ interactions between anthracene units, at multiple sites. The shapes and dynamic motions of these macrocyclic oligomers are controllable by structural modifications and interactions with external species. Further studies to obtain X-ray structures and synthesize larger oligomers are in progress.

Experimental

Melting points are uncorrected. Elemental analyses were performed with a Perkin-Elmer 2400 series analyzer. NMR spectra were measured on a Varian Gemini-300 (^{1}H: 300 MHz, ^{13}C: 75 MHz), a JEOL GSX-400 (^{1}H: 400 MHz, ^{13}C: 100 MHz), or a JEOL Lambda-500 (^{1}H: 500 MHz, ^{13}C: 125 MHz) spectrometer. High-resolution FAB mass spectra were measured on a JEOL MStation-700 spectrometer. MALDI-TOF mass spectra were measured on a Voyager-Biocad spectrometer.

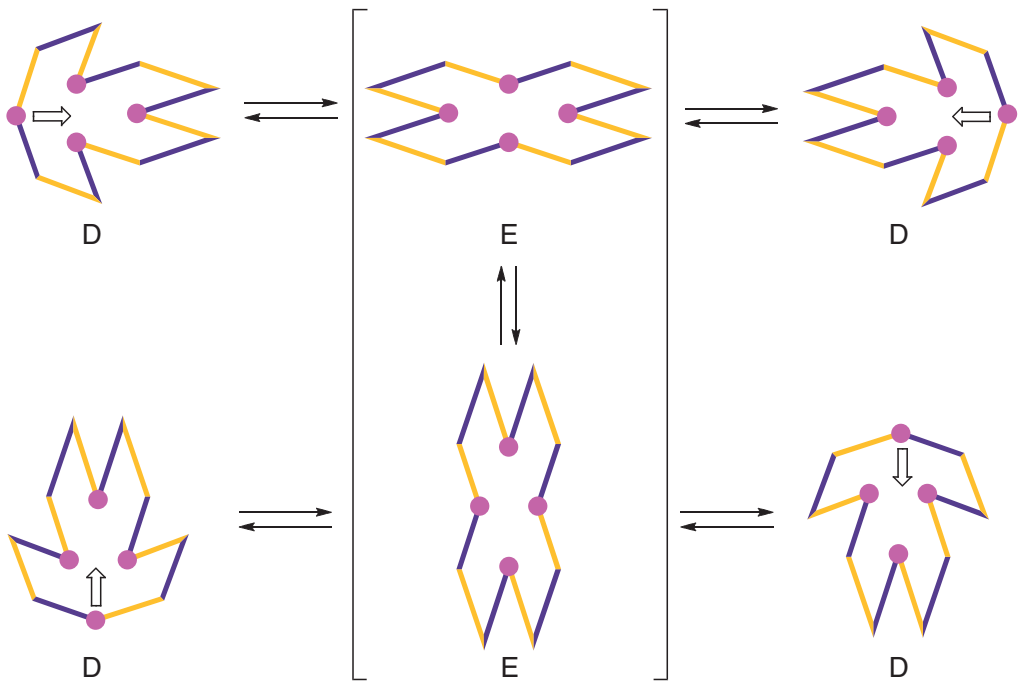

Scheme 3. Schematic of a plausible conformational pathway of **7**. Symbols **D** and **E** correspond to the structures in Figure 7. For abbreviations of building units, see Scheme 2.

GPC was performed on a Japan Analytical Industry Co. LC-908 recycling preparative HPLC system with 20 mm $\phi \times 600$ mm JAIGEL-1H and 2H columns using chloroform eluent. UV spectra were measured on a Hitachi U-3000 spectrometer with a 10 mm cell. Fluorescence spectra were measured on a JASCO FP-6500 spectrofluorometer with a 10 mm cell with a sample degassed by Ar gas immediately before measurements upon excitation at 393 nm. The fluorescence quantum yields were determined with a 9,10-diphenylanthracene sample as the standard.[13a] The fluorescence lifetimes were measured on a Spectra-Physics time-resolved spectrofluorometer system (Tsunami 3960/50-M2S) with a Ti:Sapphire laser. Column chromatography was carried out with Merck Silica Gel 60 (70–230 mesh) or Fuji Silysia Chromatorex-NH (100–200 mesh).

10-Dodecyl-1,8-diiodoanthracene (9). A solution of dodecylmagnesium bromide in ether was prepared from Mg (186 mg, 7.65 mmol), 1-bromododecane (1.91 g, 7.66 mmol), and dry ether (30 mL) in an ordinary manner. To the solution, 4,5-diiodo-9-anthrone[8] (1.14 g, 2.56 mmol) was added under N_2. The reaction mixture was stirred for 20 h at room temperature, and quenched with aq NH_4Cl. The products were extracted with ether, dried over $MgSO_4$, and evaporated. The crude product was purified by chromatography on silica gel with hexane eluent to give a yellow solid. Yield 685 mg (45%); mp 93–95 °C; ^{1}H NMR (300 MHz, $CDCl_3$): δ 0.87 (3H, t, $J = 6.4$ Hz), 1.18–1.44 (16H, m), 1.54 (2H, m), 1.77 (2H, m), 3.56 (2H, t, $J = 8.2$ Hz), 7.21 (2H, dd, $J = 9.2$, 7.1 Hz), 8.16 (2H, d, $J = 7.1$ Hz), 8.26 (2H, d, $J = 9.2$ Hz), 8.96 (1H, s); ^{13}C NMR (75 MHz, $CDCl_3$): δ 14.13, 22.68, 28.44, 29.34, 29.50, 29.65, 30.23, 31.54, 31.91, 101.53, 125.31, 126.54, 130.08, 132.81, 136.30, 137.40, 137.49 (3 alkyl signals missing); HRMS (FAB) Found m/z 598.0596, Calcd for $C_{26}H_{32}I_2$: 598.0593 $[M]^+$; Anal. Found: C, 52.41; H, 5.17%. Calcd for $C_{26}H_{32}I_2$: C, 52.19; H, 5.39%.

Trimer 11. A solution of **9** (868 mg, 1.45 mmol) and **10**[4] (1.15 g, 3.01 mmol) in triethylamine (70 mL) and THF (70 mL) was degassed by bubbling Ar gas for 1 h. To the solution were added $[Pd(PPh_3)_4]$ (175 mg, 0.15 mmol) and CuI (29 mg, 0.15 mmol), and the reaction mixture was refluxed for 48 h under Ar. The solvent was evaporated, and the crude product was purified by chromatography on silica gel with hexane/chloroform 8:1 eluent. Recrystallization from hexane/chloroform gave the desired compound as a yellow solid. Yield 1.25 g (78%); mp 146–147 °C; ^{1}H NMR (400 MHz, $CDCl_3$): δ 0.63 (6H, septet, $J = 6.9$ Hz), 0.86 (36H, d, $J = 6.9$ Hz), 0.89 (3H, t, $J = 6.9$ Hz), 1.23–1.40 (14H, m), 1.46 (2H, m), 1.64 (2H, m), 1.88 (2H, m), 3.68 (2H, t, $J = 6.7$ Hz), 6.49 (2H, dd, $J = 8.2$, 6.9 Hz), 7.33 (2H, dd, $J = 8.7$, 6.9 Hz), 7.36–7.41 (4H, m), 7.53 (2H, dd, $J = 9.1$, 6.9 Hz), 7.66 (2H, d, $J = 6.4$ Hz), 7.82–7.86 (4H, m), 8.07 (2H, s), 8.34 (2H, d, $J = 9.2$ Hz), 9.19 (2H, s), 9.97 (1H, s); ^{13}C NMR (125 MHz, $CDCl_3$): δ 11.99, 14.87, 19.13, 23.44, 28.98, 30.11, 30.38, 30.39, 30.45, 31.06, 31.55, 32.31, 32.47, 32.66, 93.06, 93.81, 96.91, 105.63, 121.37, 122.45, 123.84, 124.15, 124.72, 124.93, 125.11, 125.63, 125.85, 127.70, 128.75, 129.47, 130.16, 130.38, 131.26, 131.32, 131.57, 131.63, 132.09, 132.61, 137.07 (one aromatic signal missing); UV ($CHCl_3$): λ_{max} (ε) 255 (201000), 265 (198000), 372 (20900), 393 (28100), 415 (33500), 436 nm (27600, sh); FL ($CHCl_3$): λ_{max} 455, 482 nm, λ_{ex} 393 nm ($\Phi_f = 0.10$); HRMS (FAB): Found m/z 1106.6573, Calcd for $C_{80}H_{90}Si_2$: 1106.6581 $[M]^+$; Anal. Found: C, 86.63; H, 8.39%. Calcd for $C_{80}H_{90}Si_2$: C, 86.74; H, 8.19%.

Trimer 12. To a solution of **11** (570 mg, 0.515 mmol) in dichloromethane (215 mL) was added TBAF (0.51 mL of 1.0 mol L^{-1} THF solution, 0.51 mmol). After the solution was stirred for 1 h at room temperature, the solution was treated with water (40 mL). The organic layer was separated, dried over $MgSO_4$, and evaporated. The crude product was separated by chromatography on silica gel with hexane/chloroform 5:1 eluent to give the desired compound as a yellow solid in addition to the recovery of 25% of the starting material. Yield 271 mg (55%); mp 127–129 °C; ^{1}H NMR (400 MHz, $CDCl_3$): δ 0.54 (3H, septet, $J = 7.3$ Hz), 0.74 (18H, d, $J = 7.3$ Hz), 0.89 (3H, t, $J = 6.9$ Hz), 1.22–1.42 (14H, m), 1.46 (2H, m), 1.65 (2H, m), 1.89 (2H, m), 3.01 (1H, s), 3.68 (2H, t, $J = 8.3$ Hz), 6.58 (1H, dd, $J = 8.2$, 6.9 Hz), 6.82 (1H, dd, $J = 8.2$, 6.8 Hz), 7.13 (1H, d, $J = 6.0$ Hz), 7.20 (1H, dd, $J = 8.7$, 7.3 Hz), 7.23 (1H, dd, $J = 8.7$, 6.9 Hz), 7.47–7.62 (7H, m), 7.71 (1H, d, $J = 8.2$ Hz), 7.75 (1H, d, $J = 8.2$ Hz), 7.90 (1H, d, $J = 6.4$ Hz), 7.91 (1H, d, $J = 6.8$ Hz), 8.03 (2H, s), 8.34 (1H, d, $J = 6.4$ Hz), 8.36 (1H, d, $J = 8.2$ Hz), 9.30 (1H, s), 9.33 (1H, s), 10.10 (1H, s); ^{13}C NMR (125 MHz, $CDCl_3$): δ 11.18, 14.18, 18.46, 18.64, 22.74, 28.44, 29.39, 29.67, 29.74, 30.44, 31.74, 31.92, 81.54, 82.60, 92.85, 93.12, 93.18, 93.43, 96.21, 104.93, 120.47, 120.92, 120.98, 121.76, 122.98, 123.01, 123.70, 123.73, 123.99, 124.22, 124.30, 124.38, 124.61, 125.04, 125.13, 125.24, 126.63, 127.02, 127.95, 128.27, 128.68, 128.89, 129.47, 129.49, 129.68, 129.82, 129.94, 130.50, 130.60, 130.67, 130.74, 130.77, 130.84, 130.92, 130.96, 131.06, 131.49, 131.65, 131.81, 136.59 (2 aromatic signals missing); HRMS (FAB) Found m/z 950.5202, Calcd for $C_{71}H_{70}Si$: 950.5247 $[M]^+$; Anal. Found: C, 89.88; H, 7.63%. Calcd for $C_{71}H_{70}Si$: C, 89.63; H, 7.42%.

Hexamer 13. To a solution of **12** (696 mg, 0.732 mmol) in diisopropylamine (50 mL) and THF (50 mL) were added $[PdCl_2(PPh_3)_2]$ (27.7 mg, 40 μmol), CuI (14.0 mg, 74 μmol), and I_2 (97.6 mg, 0.385 mmol). The reaction mixture was stirred for 16 h at room temperature. The solvent was evaporated, and the crude product was purified by chromatography on silica gel with hexane/chloroform 3:1 eluent to give the desired compound as a yellow solid. Yield 627 mg (90%); mp 230–231 °C; ^{1}H NMR (400 MHz, $CDCl_3$): δ 0.44 (6H, septet, $J = 6.9$ Hz), 0.61 (36H, d, $J = 6.9$ Hz), 0.91 (6H, t, $J = 6.9$ Hz), 1.20–1.33 (40H, m), 2.41 (4H, m), 6.15 (2H, t, $J = 7.9$ Hz), 6.25 (2H, t, $J = 7.5$ Hz), 6.73 (2H, d, $J = 8.7$ Hz), 6.76 (2H, d, $J = 6.4$ Hz), 6.85 (2H, t, $J = 7.8$ Hz), 7.12 (2H, t, $J = 8.2$ Hz), 7.18 (2H, d, $J = 5.9$ Hz), 7.22 (2H, m), 7.31 (2H, dd, $J = 8.7$, 6.9 Hz), 7.39 (2H, d, $J = 8.7$ Hz), 7.46 (2H, d, $J = 6.9$ Hz), 7.53 (4H, d, $J = 7.3$ Hz), 7.60 (2H, d, $J = 6.3$ Hz), 7.66–7.70 (4H, m), 7.76 (2H, d, $J = 6.8$ Hz), 7.84 (2H, d, $J = 8.7$ Hz), 7.95 (2H, s), 8.09 (2H, s), 8.44 (2H, s), 9.28 (2H, s), 9.77 (2H, s); UV ($CHCl_3$): λ_{max} (ε) 253 (310000), 393 (45900), 416 (52800), 449 nm (45500); FL ($CHCl_3$): λ_{max} 513 nm, λ_{ex} 393 nm ($\Phi_f = 0.05$, $\tau_f = 2.9$ ns); HRMS (FAB): Found m/z 1899.0304, Calcd for $C_{142}H_{138}Si_2$: 1899.0337 $[M]^+$; Anal. Found: C, 89.86; H, 7.30%. Calcd for $C_{142}H_{138}Si_2$: C, 89.73; H, 7.32%.

Macrocyclization of 13. *Method 1*: To a solution of **13** (106 mg, 56 μmol) in THF (50 mL) was added TBAF (0.12 mL of 1.0 mol L^{-1} THF solution, 0.12 mmol). After the solution was stirred for 30 min at room temperature, the solvent was evaporated. The residue was dissolved in pyridine (15 mL), and $Cu(OAc)_2 \cdot H_2O$ (278 mg, 1.40 mmol) and CuCl (111 mg, 1.12 mmol) were added. The reaction mixture was stirred for 5 h at 60 °C. After the solvent was mostly evaporated, the residual solid was subjected to chromatography on silica gel (NH) with chloroform eluent to remove copper reagents. The residue was crystallized from toluene to give pure hexamer **6a** (18 mg, 20%) as yellow crystals. The filtrate was further purified by GPC with chloroform eluent to give a small amount of **7a** (ca. 1 mg, 1%).

Method 2: To a solution of **13** (93 mg, 49 μmol) in THF (53 mL) was added TBAF (0.12 mL of 1.0 mol L^{-1} THF solution, 0.12 mmol). After the solution was stirred for 30 min at room temperature, the solvent was evaporated. The residue was dissolved in diisopropylamine (2.0 mL) and THF (8.0 mL). To the solution was added $[PdCl_2(PPh_3)_2]$ (7.7 mg, 11 μmol), CuI (2.5 mg, 13 μmol), and I_2 (4.7 mg, 19 μmol). After the reaction mixture was stirred for 15 h at room temperature, the solvent was evaporated. The residual solid was subjected to chromatography on silica gel (NH) with hexane/chloroform 2:1 eluent. The easily eluted fraction ($R_f = 0.43$ hexane/chloroform 2:1) was hexamer **6a**, which was further purified by recrystallization from hexane/chloroform to give 17 mg (22%) of pure material as a yellow solid. The less easily eluted fraction ($R_f = 0.18$ hexane/chloroform 2:1) mainly contained cyclic dodecamer **7a**, which was purified by GPC with chloroform eluent to give 5.1 mg (7%) of practically pure material as a yellow solid.

Cyclic Hexamer 6a: mp 295–298 °C (dec); ^{1}H NMR (400 MHz, $CDCl_3$): δ 0.88 (6H, m), 1.07–1.35 (40H, m), 2.17 (4H, m), 6.45 (4H, dd, $J = 7.9$, 8.6 Hz), 6.78 (4H, dd, $J = 6.4$, 8.6 Hz), 6.95 (4H, d, $J = 8.4$ Hz), 7.14 (4H, d, $J = 6.4$ Hz), 7.40 (4H, dd, $J = 6.8$, 8.8 Hz), 7.64 (4H, d, $J = 6.4$ Hz), 7.88 (4H, d, $J = 8.8$ Hz), 7.99 (4H, d, $J = 6.4$ Hz), 8.09 (4H, d, $J = 6.4$ Hz), 8.47 (4H, s), 9.40 (4H, s), 9.56 (2H, s); UV ($CHCl_3$): λ_{max} (ε) 265 (38400), 432 (65300), 458 nm (46000); FL ($CHCl_3$): λ_{max} 502 nm, λ_{ex} 393 nm ($\Phi_f = 0.10$, $\tau_f = 4.5$ ns); HRMS (FAB): Found m/z 1584.7491, Calcd for $C_{124}H_{96}$: 1584.7546 $[M]^+$; Anal. Found: C, 93.55; H, 6.01%. Calcd for $C_{124}H_{96}$: C, 93.90; H, 6.10%.

Cyclic Dodecamer 7a: mp 276–288 °C (dec); ^{1}H NMR (400 MHz, $CDCl_3$, 60 °C): δ 0.68 (8H, brm), 0.98 (12H, m), 1.08–1.45 (72H, m), 1.63 (8H, m), 6.63–6.69 (16H, m), 6.75 (8H, d, $J = 8.8$ Hz), 6.90 (8H, t, $J = 7.2$ Hz), 6.96 (8H, d, $J = 6.4$ Hz), 7.02 (8H, d, $J = 6.8$ Hz), 7.48 (8H, d, $J = 8.8$ Hz), 7.61 (8H, d, $J = 8.3$ Hz), 7.73 (8H, d, $J = 6.4$ Hz), 7.95 (8H, s), 8.76 (8H, s), 9.76 (4H, s); UV ($CHCl_3$): λ_{max} (ε) 258 (616000), 425 (96700), 462 nm (sh, 56000); FL ($CHCl_3$): λ_{max} 516 nm, λ_{ex} 393 nm ($\Phi_f = 0.04$, $\tau_f = 4.5$ ns); MS (MALDI-TOF): Found m/z 3169.86, Calcd for $C_{248}H_{192}$: 3169.50 $[M]^+$.

DFT Calculations. The DFT calculations were carried out with Gaussian 09W[18] on a Windows computer. The structures were optimized by hybrid DFT at the M05/3-21G level from several input structures.

This work was partly supported by Grants-in-Aid for Scientific Research (C) No. 19550054 and for Scientific Research on Innovative Areas (Integrated Organic Synthesis) No. 22106543 from MEXT (Ministry of Education, Culture, Sports, Science and Technology, Japan) and by a matching fund subsidy for private universities from MEXT.

References

1 Part 18 of the series: T. Ishikawa, T. Iwanaga, S. Toyota, M. Yamasaki, *Bull. Chem. Soc. Jpn.* **2011**, *84*, 729.

2 a) *Poly(arylene ethynylene)s: From Synthesis to Application* in *Advances in Polymer Science*, ed. by C. Weder, Springer, Heidelberg, **2005**, Vol. 177. doi:10.1007/b101353. b) T. Kawase, H. Kurata, *Chem. Rev.* **2006**, *106*, 5250. c) T. Kawase, *Synlett* **2007**, 2609. d) K. Tahara, Y. Tobe, *Chem. Rev.* **2006**, *106*, 5274. e) E. L. Spitler, C. A. Johnson, II, M. M. Haley, *Chem. Rev.* **2006**, *106*, 5344. f) W. Zhang, J. S. Moore, *Angew. Chem., Int. Ed.* **2006**, *45*, 4416. g) S. Höger, *Chem.—Eur. J.* **2004**, *10*, 1320.

3 S. Toyota, *Chem. Lett.* **2011**, *40*, 12.

4 a) S. Toyota, M. Goichi, M. Kotani, *Angew. Chem., Int. Ed.* **2004**, *43*, 2248. b) S. Toyota, M. Goichi, M. Kotani, M. Takezaki, *Bull. Chem. Soc. Jpn.* **2005**, *78*, 2214.

5 S. Toyota, T. Kawakami, R. Shinnishi, R. Sugiki, S. Suzuki, T. Iwanaga, *Org. Biomol. Chem.* **2010**, *8*, 4997.

6 a) P. Kissel, J. van Heijst, R. Enning, A. Stemmer, A. D. Schlüter, J. Sakamoto, *Org. Lett.* **2010**, *12*, 2778. b) P. Kissel, A. D. Schlüter, J. Sakamoto, *Chem.—Eur. J.* **2009**, *15*, 8955. c) K. Miki, M. Fujita, Y. Inoue, Y. Senda, T. Kowada, K. Ohe, *J. Org. Chem.* **2010**, *75*, 3537.

7 a) S. Toyota, H. Miyahara, M. Goichi, S. Yamasaki, T. Iwanaga, *Bull. Chem. Soc. Jpn.* **2009**, *82*, 931. b) S. Toyota, H. Miyahara, M. Goichi, K. Wakamatsu, T. Iwanaga, *Bull. Chem. Soc. Jpn.* **2008**, *81*, 1147.

8 a) M. Goichi, K. Segawa, S. Suzuki, S. Toyota, *Synthesis* **2005**, 2116. b) J. M. Lovell, J. A. Joule, *Synth. Commun.* **1997**, *27*, 1209.

9 a) S. Toyota, S. Suzuki, M. Goichi, *Chem.—Eur. J.* **2006**, *12*, 2482. b) S. Toyota, M. Kurokawa, M. Araki, K. Nakamura, T. Iwanaga, *Org. Lett.* **2007**, *9*, 3655.

10 a) Q. Liu, D. J. Burton, *Tetrahedron Lett.* **1997**, *38*, 4371. b) J. A. Marsden, M. J. O'Connor, M. M. Haley, *Org. Lett.* **2004**, *6*, 2385.

11 a) P. Siemsen, R. C. Livingston, F. Diederich, *Angew. Chem., Int. Ed.* **2000**, *39*, 2632. b) J. A. Marsden, M. M. Haley, *J. Org. Chem.* **2005**, *70*, 10213.

12 J. A. Marsden, J. J. Miller, L. D. Shirtcliff, M. M. Haley, *J. Am. Chem. Soc.* **2005**, *127*, 2464.

13 a) B. Valeur, *Molecular Fluorescence: Principles and Applications*, Wiley-VCH, Weinheim, **2002**, Chap. 3. b) P. Rademacher, in *Modern Cyclophane Chemistry*, ed. by R. Gleiter, H. Hopf, Wiley-VCH, Weinheim, **2004**, Chap. 11.

14 a) Y. Morisaki, T. Murakami, T. Sawamura, Y. Chujo, *Macromolecules* **2009**, *42*, 3656. b) W.-L. Wang, J. Xu, Z. Sun, X. Zhang, Y. Lu, Y.-H. Lai, *Macromolecules* **2006**, *39*, 7277.

15 a) Y. Zhao, D. G. Truhlar, *Chem. Phys. Lett.* **2011**, *502*, 1. b) Y. Zhao, D. G. Truhlar, *Acc. Chem. Res.* **2008**, *41*, 157.

16 a) C. A. Hunter, J. K. M. Sanders, *J. Am. Chem. Soc.* **1990**, *112*, 5525. b) C. Gonzalez, E. C. Lim, *J. Phys. Chem. A* **2000**, *104*, 2953. c) C. Gonzalez, E. C. Lim, *J. Phys. Chem. A* **2003**, *107*, 10105. d) R. Podeszwa, K. Szalewicz, *Phys. Chem. Chem. Phys.* **2008**, *10*, 2735.

17 M. Nishio, M. Hirota, Y. Umezawa, *The CH/π Interaction: Evidence, Nature, and Consequences*, Wiley-VCH, New York, **1998**.

18 M. J. Frisch, G. W. Trucks, H. B. Schlegel, G. E. Scuseria, M. A. Robb, J. R. Cheeseman, G. Scalmani, V. Barone, B. Mennucci, G. A. Petersson, H. Nakatsuji, M. Caricato, X. Li, H. P. Hratchian, A. F. Izmaylov, J. Bloino, G. Zheng, J. L. Sonnenberg, M. Hada, M. Ehara, K. Toyota, R. Fukuda, J. Hasegawa, M. Ishida, T. Nakajima, Y. Honda, O. Kitao, H. Nakai, T. Vreven, J. A. Montgomery, Jr., J. E. Peralta, F. Ogliaro, M. Bearpark, J. J. Heyd, E. Brothers, K. N. Kudin, V. N. Staroverov, R. Kobayashi, J. Normand, K. Raghavachari, A. Rendell, J. C. Burant, S. S. Iyengar, J. Tomasi, M. Cossi, N. Rega, J. M. Millam, M. Klene, J. E. Knox, J. B. Cross, V. Bakken, C. Adamo, J. Jaramillo, R. Gomperts, R. E. Stratmann, O. Yazyev, A. J. Austin, R. Cammi, C. Pomelli, J. W. Ochterski, R. L. Martin, K. Morokuma, V. G. Zakrzewski, G. A. Voth, P. Salvador, J. J. Dannenberg, S. Dapprich, A. D. Daniels, Ö. Farkas, J. B. Foresman, J. V. Ortiz, J. Cioslowski, D. J. Fox, *Gaussian 09 (Revision B.01)*, Gaussian, Inc., Wallingford CT, USA, **2009**.